MAGELLAN PROJECT

University of Arizona | Carnegie Institution of Washington | The Johns Hopkins University

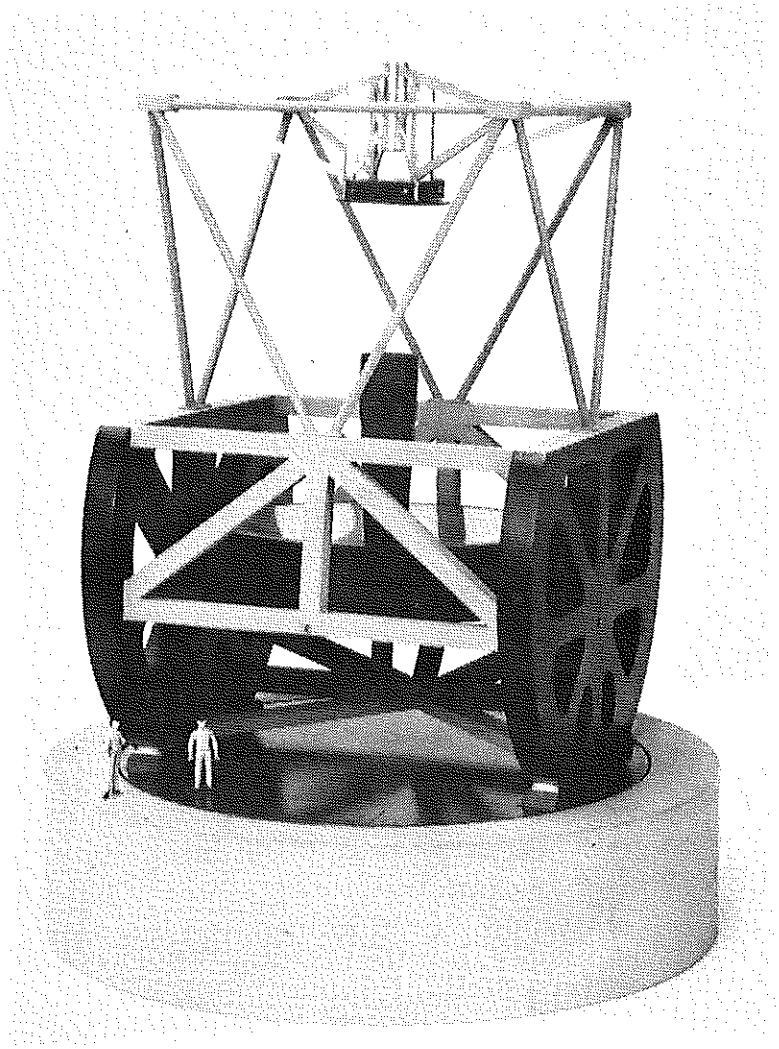

Las Campanas Observatory Seeing Measurements

S. E. Persson, D. M. Carr, and J. H. Jacobs
The Observatories of the
Carnegie Institution of Washington
Pasadena, California

December 1989
No. 14

ABSTRACT

Instrumentation built to record seeing data automatically via image motion measurements of bright stars in small telescopes is described. The centroid of the star image is found 256 times per second in one dimension and is analyzed on-line. The device works over a range of FWHM values as would be seen through a large telescope between <0.1 and 3.0 arcseconds. The first results for two identical instruments set up at two locations near the duPont Telescope at Las Campanas Observatory are reported. For a total of 61 nights of data (450 hours at each site), the median seeing is 0.6 arcseconds, with quartiles at 0.4 and 0.8 arcseconds. These are FWHM values referred to 5000 Å at the zenith. So far, the two sites are indistinguishable on average.

I. INTRODUCTION

The quality of the astronomical seeing is certainly one of the most important parameters characterizing a telescope site. In recent years there has been a growing recognition that stellar image diameters generally delivered to the focal plane instrumentation of most large telescopes are severely degraded by thermal effects in the dome and around the telescope itself, and much effort has gone into more recent telescope and dome designs to attempt to improve this situation. Assuming that future telescopes and domes will indeed largely defeat the locally caused seeing effects, the selection of an excellent site in the first place takes on even more importance, not only for scientific reasons, but for issues of telescope engineering and control design as well. Thanks to the efforts 25 years ago of a number of experienced astronomers, notably Babcock and Irwin, the Las Campanas Observatory was built at what appeared to be a very promising site. Observations carried out on our telescopes there have generally borne out the expectations of good seeing, but there has been as yet no quantitative data on its distribution with windspeed or season, on the "speed" of the seeing blur, or on the deleterious thermal effects of the domes.

The Carnegie Institution of Washington plans in the next few years to build an 8-m telescope within the boundaries of the present observatory. It was decided that in order to be absolutely certain that the best local site was selected for the 8-m telescope it was necessary to carry out a seeing survey. Because the primary goal was to select the best site among several within only a few km of each other, what is needed is a high–sensitivity measurement of the seeing, and one that operates well when the seeing is at its best. The purpose of the present paper is to describe the philosophy, apparatus, operation and first results of this survey. We have built equipment that gives both relative and absolute seeing data on a routine basis.

We hoped to accomplish several goals in measuring the seeing at Las Campanas:

(1) Distinguish which of three potential sites offered the best overall (median) seeing. These sites were chosen for logistical and topographic reasons. Early data on microthermal activity indicated differences from site to site, but we wanted a new, extensive, and calibrated data set to be certain that we placed the 8-m telescope at the best site, should significant differences be found.

(2) Establish, over a period of several years, the distribution of absolute seeing values so that we and perhaps future telescope builders could engineer their telescopes, optical components, instrumentation, and control systems with realistic optical and mechanical performance goals in mind. It would be a waste of a good site to build a telescope that delivered images comparable to the median seeing. By converting all of Babcock and Irwin's (1987) stellar image motion data for four Chilean sites to FWHM values we showed (Persson, Babcock, and Irwin 1987) that the median value at La Silla ought to be roughly 0.7" FWHM. The same should be be true of Las Campanas.

(3) Have available, on a more or less routine basis, quantitative data on the instantaneous value of the seeing independent of any degrading influences of domes and heavy telescope structures. With this information we expect understand how well our efforts at improving the seeing within our existing telescope domes have actually worked. Such procedures as cooling the observing room floor, and ventilating the dome and telescope are known to be effective, but quantitative comparisons are needed.

(4) Be able to inform workers interested in adaptive optics and interferometry just what fraction of the time the seeing is better than some interesting limit, and what the distribution of the good seeing episodes is like, when they occur, how long they last, etc.

The good-seeing tail of the distribution of seeing values is critical in deciding how hard to work at stabilizing the image, because poor images cannot be significantly improved, but spectacular gains should be realizable, especially at infrared wavelengths, if one is dealing with images around 0.5" FWHM.

(5) Finally, have available an independent measure of the external seeing when we begin to install and tune up the 8-m telescope of the Magellan Project.

As is well known, there are many methods available to estimate image quality, or to distinguish two sites on a relative basis. It was decided that measurements of the image motion of stars in small telescopes would yield data in a form that is most directly comparable to the sizes and shapes of images seen through a large telescope. Furthermore, techniques of image motion measurement have been widely used in recent years and data from a number of different sites are becoming available. In order to conduct a survey at a remote site such as Las Campanas it was thought essential to build simple and virtually automatic devices. Before describing the equipment we first give a very short summary of the theory behind the measurements.

II. PRINCIPLES of OPERATION

A wavefront that is flat at the top of the atmosphere will enter the telescope considerably warped by virtue of its passage through a turbulent atmosphere containing a distribution of cells of differing size and refractive index. These cells move rapidly across the light path, due to winds at various heights above the dome, convection in and above the dome, off the surface of the primary and telescope structure, the ground around the dome, and so forth. Over some characteristic scale at the telescope objective one can define a size over which the rms phase change of the wavefront is less than one radian; this piece of the wavefront is essentially only tilted with respect to the average direction of light propagation. Intuitively, one can see that a (perfect) small telescope that intercepts this piece of the wavefront delivers a diffraction-limited image that only shifts in the focal plane. As the coherent patches move rapidly around within the large telescope objective, the small telescope sees rapid image wander. In bad seeing the size of the coherent region will be smaller and the tilts will be larger, leading to larger rms image motions in the small telescope, and a larger FWHM for long exposure images seen in a large telescope. This is the basis of image motion measurements designed to estimate the seeing expected in a large telescope. The theory has been developed by Fried (1965, 1966), Young (1974), and others; the subject has been reviewed by Woolf (1982).

Several recent papers have reviewed and developed the theory of image motion measurement as actually applied in the case of one or two telescopes, and we shall not repeat it here. Papers that are particularly useful in this regard are those of Woolf (1982), Moroder and Righini (1973), Forbes and Woolf (1983), Woolf and Ulich (1983), Angel (1987), Martin (1987), and Sarazin and Roddier (1989). Martin (1987) has given a review of techniques, and an important caution regarding sampling time for double and single-telescope measurements of image motion. For the purposes of explaining the principles that led to the design of our instrument, it is sufficient to quote the equations that we have used from the above references.

The relationship between rms image motion as recorded in a telescope of aperture diameter d, and the region size r_o (Fried's parameter) is approximately

$$r_o = \left[\frac{6.88}{\langle\alpha^2\rangle(2\pi/\lambda)^2 d^{1/3}}\right]^{3/5} \tag{1}$$

where α is the one-dimensional angular image motion in radians, and the measurements are carried out at wavelength λ (Moroder and Righini 1973).

The fundamental parameter r_o – the "coherence diameter" – can be thought of as the diameter of a small (perfect) telescope whose diffraction limited FWHM image diameter is (approximately) equal to the "seeing" image size θ as recorded in a long exposure image through a large telescope. Thus r_o is related to θ (the FWHM) as

$$\theta = 0.98\lambda/r_o \tag{2}$$

and is independent of the large telescope aperture diameter D. The units of r_o are (conventionally) cm. A convenient rule of thumb is

$$\theta(arcsec) = 10cm/r_o \tag{3}$$

which applies at a wavelength of 5000 Å. The parameter r_o scales with wavelength as

$$r_o(\lambda_2) = r_o(\lambda_1) \times (\lambda_2/\lambda_1)^{1.2} \tag{4}$$

The seeing in the large telescope thus improves slowly with wavelength: $\theta \propto \lambda^{-0.2}$.

Values of r_o in the near-infrared can become very large if the seeing is excellent in the visible. For example, in 0.5" seeing at V, r_o in the K band (2.2μm) will be 105 cm. It is this rapid scaling of r_o with wavelength that has led to efforts to sense and correct the wavefront tilts before recording images, because the number of sensors and actuators needed to flatten the wavefront over the area of the large telescope objective scales as $\lambda^{-2.4}$.

It is well known that the seeing deteriorates with increasing airmass. From theory one expects a scaling of the form

$$\theta(secZ) = \theta(1.00) \times (secZ)^{0.6} \tag{5}$$

The wind at various heights above the site blows the turbulent elements across the light path in a coherence timescale $\tau_c \approx r_o/V_{wind}$. In order not to suppress high frequency components of the image wander recorded in our small telescope, we must sample the image location at a frequency several times $1/\tau_c$, which for a windspeed of 20 mph = 9 m s^{-1} and r_o = 10 cm ("1 arcsecond seeing"), is 90 Hz. Martin (1987) has given detailed computations of the effects of neglecting the high frequency components; his results show that completely erroneous conclusions can be drawn about the distribution of r_o values if, for example, one cuts off the frequency response at the convenient value of 30 Hz. Fortunately both theory and experiment indicate that the power spectra of image motion typically fall fairly rapidly toward higher frequencies, so one could in principle correct for the missing components. We shall return to this point later.

The above brief summary is sufficient for an explanation of the workings of the equipment we built to evaluate the seeing at Las Campanas. Readers interested in the details should consult the papers by Fried (1965), Young (1974), Woolf (1987), Martin (1987), and references therein.

III. APPARATUS and OPERATION

a) Instrumentation

The principle of operation is to measure the position of a stellar image by rapidly shifting it between two detectors, in such a way that a perfectly centered image would spend exactly half its time on each detector. The difference in time spent on the two detectors is linearly proportional to the displacement from the central position. Figure 1 shows a schematic diagram of the optical/mechanical device. Light from a star enters a 7-inch diameter Questar telescope. The Questar 7 Maksutov telescope was chosen for its excellent optical quality and high throughput; enhanced aluminum coatings on the mirrors were specified. At the nominal f/13.5 focus (the scale is 85 "/mm) the images are (supposed to be) nearly diffraction limited. Seeing surveys in the north make use of Polaris, but in the south it is necessary to track the stars being measured. The Questar is mounted on a precision drive that makes use of a Byers 11.4–inch diameter RA gear. The Byers gear sets are favored by amateur astronomers for their high precision and lack of jitter. The drive is a simple commercial unit used by amateur astronomers, and was found to perform well.

The next element in the optical path is a calibration plate, to which all the image motion measurements are ultimately referred; its operation is explained below. After passing through the calibration plate the light reflects off a small mirror (6.4 mm in diameter) which is mounted on a piezo-electric bimorph purchased from the EDO Corporation (Salt Lake City). A piezo-electric bimorph is constructed so that it bends as voltages are applied across it, and in so doing the mirror is tilted such that the image of the star is swept across the knife-edge mirror. The light converges to a focus at this knife-edge, which is itself a mirror. If the star image lands precisely on the knife-edge mirror, then half the light will be reflected to the field lens plus photomultiplier tube marked PMT2, the other half passing by to PMT1. The quality of the edge of the knife-edge is important; these were custom made. The unvignetted field of the PMTs is set by the size of the small mirror mounted on the piezo; it is about 140" in diameter.

Figure 2 shows a schematic timing diagram. The piezo is driven with a triangular wave so that the star image is swept at a constant rate across the knife edge, which is located precisely at the focus of the telescope. The triangle wave is generated using an Intersil 8038 function generator chip, followed by a filter to round off the peaks (this is explained below). It is then amplified using a Burr-Brown model 3583 fast high-voltage opamp to convert low- level drive signals to the $\pm$ 100 volt swings needed to move the piezo. As the mirror oscillates, the star image either lands on the knife-edge mirror or it misses it; it is thus alternately directed either to PMT1 or PMT2, as indicated in panel 2 of Figure 2. Field lenses are used to image the telescope objective onto the photosurface of the PMTs, as is usually the practice in photoelectric photometers. The output currents of the two PMTs are converted to voltages, which are sensed at the two inputs of a precision voltage comparator. The output of this comparator swings high or low at the precise instant that one voltage exceeds the other, which for a perfect mirror and identical PMTs occurs when the centroid of the star image is exactly at the knife-edge. The PMT signals are smoothed with a 2.2 kHz low-pass filter to eliminate high frequency noise which could

cause multiple detections of the edge. The comparator output voltage is then converted to TTL levels, and these are used to gate two counters, which count TTL pulses generated by a 5 MHz crystal clock. Because the triangular wave is linear over the central two-thirds of its travel, the total number of pulses counted between zero crossings of the voltage comparator is linearly proportional to the one-dimensional displacement of the star from the nominal central position. This device is essentially an analog position-to-digital converter, which produces a digital position measurement very early in the overall signal/data chain.

By inspection of the raw photomultiplier signals one sees the scintillation (stellar brightness variations) that would play havoc with such a device if it did not centroid the star fast enough. It takes about 25 μsec for the core of the star image to sweep past the knife-edge, which is much faster than scintillation variations. Inspection of the digitized output position shows a smooth function, with no evidence for scintillation noise.

The parameters of the setup finally adopted are as follows: The peak-to-peak travel of the star image due to the piezo/mirror is 15 arcsec peak-to-peak and the chopping frequency is 256 Hz. We found a resonance in the piezos when we tried to drive them with a sharp triangle wave. We rolled off some of the higher harmonics of the driving signal with four-pole Bessel filters, and settled on a chopping frequency that fell between resonances. These two steps prevent excitation of the resonant frequencies of the piezo by the driving wave and its harmonics. The input waveform to the piezo/mirror is linear to within less than one percent over 80 % of the travel around center.

The photomultiplier tubes are RCA type 4516, which have peak response at a wavelength of 4400 Å, and an effective bandwidth of 1500 Å. The quantum efficiency at peak is about 25 %. They are run at ambient temperature, with a cathode voltage of – 1000 V. The output currents produce voltage drops across precision resistors. The two phototube operating voltages, and hence the (signal) photo-currents are balanced by looking at the direct PMT outputs with the star falling completely on one or the other, and then adjusting their operating voltages to give equal signals. A small imbalance in the PMT outputs corresponds to a small and constant shift in the effective centroid of the star image. The operating point of the PMTs was adjusted to give about 10 volts output for the brightest star (Sirius; B = –1.45). For the bright blue stars observed neither the dark current nor the sky signal are important, and in any case the PMTs are used in such a way that large but constant additive signals would be irrelevant.

The throughput of the entire system was measured and found to lie within about 30 % of that expected for the tube performance, mirrors, coated surfaces, etc, in the light beam.

The knife-edge projects east-west on the plane of the sky, so that telescope drive irregularities and periodic errors of any frequency only cause a shift of the star image parallel to the knife-edge. Such shifts are absent in the output signal, because the location of the star along the knife-edge makes no difference to the centroid location electronics. Auto guiding in declination is accomplished by monitoring the average level of the output digitized signal, and applying appropriate corrections with the data recording subroutine turned off. In practice the star is kept within $\pm$ 3 arcseconds of the nominal center. The usable field of the instrument is greater than one arcminute, so guiding in RA (along the knife-edge) does not need to be done very often; it is done each time a calibration is done, i.e., every 10 minutes. In order to do so, we installed a solenoid-operated blade that is caused to cut into the beam, about 1 inch ahead of PMT2. The blade location is adjusted so that when it is in the beam, only half the light reaches PMT2, and the resulting signal is directly compared with half of the signal from PMT1 (both signals are chopped so

average signals are generated). If the telescope is not centered in RA one of these signals will exceed the other; these two signals feed a voltage comparator, whose output is high or low depending on the sense of the input voltage difference. The telescope is driven east or west until the two signals flip the voltage comparator, which then turns off the drive corrector. Thus once the telescope is pointed at a star it will remain pointed for several hours, and the operation is completely automatic.

b) Calibration

The quartz calibration plate (see Figure 1) determines the response of the instrument, which depends weakly on telescope focus and other factors. We describe below how the rms image motions are calculated and stored. At the conclusion of a 10-minute data set, which is also the start of the next one, a motor-driven cam causes the plate to oscillate in a quasi-sinusoidal fashion with a frequency of 10 Hz, and an amplitude that produces an *additional* motion of the star image at the focal plane of 3" peak-to-peak. This adds, in quadrature, a known component to the image motion due to the seeing. Suppose that we have calculated the rms image motion S with the calibration off, and C with it turned on. Let R = S/C. The known component due to the wobble plate is W = 3"/2$\sqrt{2}$, which is the rms value of our 3" peak-to-peak sine wave. The quadrature sum is

$$C^2 = S^2 + W^2, or \quad R^2 + (W/C)^2 = 1$$

which may be rewritten as

$$S = W R(1 - R^2)^{-1/2} \tag{6}$$

Equation (6) for the rms stellar image motion S is now in terms of the known quantity W and the measured dimensionless parameter R which is the ratio of the raw rms signals with the calibration turned off and on. The actual value of W was determined in the laboratory by measuring the thickness, refractive index, and amplitude of the cam-driven wobbler with a laser beam reflected off the surface of the quartz plate. The uncertainty in W is about ± 2 %. Note that if the seeing is really bad (such that $1 - R^2$ is negative), S is set equal to W.

The calibration technique is virtually identical to that implemented by Babcock and Irwin (1987).

c) Operator's Duties

The sequence of operations is as follows. The operator first centers a bright star (magnitude < 2) in the eyepiece using the small flip mirror. He then looks at the raw output signal from one of the PMTs with the triangle wave on. Best telescope focus corresponds to the sharpest transitions on and off the star. It is important, but not critical to keep the telescope in focus, as the centroid will be found even if the image is out of focus. He then looks at the output of the voltage comparator which is a voltage change of fixed amplitude that shifts back and forth along the time axis depending on the stellar image motion. He centers the transition on the oscilloscope screen by guiding the telescope north-south, then turns on the auto guiding feature which uses the first few seconds worth of data to establish the zero position. The system is then left tracking for several hours while data are accumulated automatically.

d) Data Processing

The operation of the instrument from this stage on is under computer control and all the following steps are carried out with no operator intervention. The on-line data processing proceeds as follows. The output pulse trains (one every 1/512 second, approximately) are counted by a counter card within an IBM PC clone computer. Twice every 1/256 second, an array element is filled with the number of pulses counted while the gate is open; this measures the position of the star at that time. Integrations last for one second. During the next second, the array of numbers is processed in several ways as described next. Data are accumulated and processed for intervals of 10 minutes, so that approximately 600 × 256 data points are collected and processed, before the next calibration is performed.

Before beginning a data sequence, the calibration plate drive is turned on for ten seconds. The rms value of C is determined from the ten (calibration) arrays of accumulated position data numbers. Next, the plate drive is turned off, the autoguiuder centers the star in both coordinates, and the accumulation of stellar data commences, at a rate of 256 (16-bit) numbers per second. The rms values of S and thus R are found, and using the stored value of C, equation (6) is solved for the rms image motion in arcseconds. Secant Z is computed from the known position of the star being measured, and values of r_o and θ from equations (1), (4) and (5) are computed and displayed on the computer screen. These change every second.

In alternate seconds different computer storage locations are used so that the computer can calculate (in background) both the rms value and the power spectrum of the previous data array. We used a Microway assembly language FFT routine that computes a 256-point FFT and its power spectrum in 100 msec. This power spectrum can be displayed on the screen (which slows down the system), or simply stored. It was found that the duty cycle could approach 100 % by restricting the FFT to a 256-point computation. After ten minutes of data have been accumulated, the system has computed 580 rms values of the image motion and corresponding r_o values, and 580 power spectra. Rather than store all this information, the r_o values are converted to θs, and these are binned into a histogram (0.05 arcsec intervals) and stored. Only the average power spectrum of the 580 that were measured is stored.

Figure 3 shows a flowchart of the data processing and recording. The final data are written on floppy disks and returned to the Observatories offices for analysis.

A few other details of the operation are as follows. For the first 64 seconds the (north-south) autoguider is not allowed to operate and the average position of the star is recorded each second. These data are later used to evaluate the slowest components of the power spectrum of image motion, to which the system is otherwise insensitive. These data do, of course, contain spurious components due to imperfect telescope tracking in declination.

The transfer function of the frequency response of the instrument is not flat out to 256 Hz. This function was determined in the lab by injecting a constant amplitude sinewave into the counter gate, thus mimicking a star image moving at a discrete frequency, and measuring the amplitude of the power spectrum as a function of frequency. Figure 4 shows the resulting function, which artificially reduces the high frequency components of the image motion. We correct for this by dividing the raw power spectrum by the normalized transfer function, and then comparing the sums of the raw and divided power spectrum components. The ratio of these, f, is used to calculate a correction factor to r_o, which depends on $f^{0.6}$. This is because r_o is proportional to the $[(\text{rms position})^2]^{-0.6}$ from equation (1), and the $(\text{rms position})^2$ is proportional to the sum of the power spectrum

components. Typically the power spectrum falls off with frequency fast enough that the correction factor amounts to between 12 and 15% in r_o. Thus the final image motion values of r_o are valid for frequencies between 2 and about 200 Hz, beyond which the correction is large enough to compromise the validity of the results.

e) Uncertainties and Systematics

One basic test of the apparatus was made to verify that electronic sources of noise were negligible, and that in fact the whole concept was reliable. A (fixed) light source was set up in the seeing tower and the system was operated as if it were measuring a star. The derived values of r_o were around 200 cm, indicating that all sources of system noise together contribute 0.05 arcsec (in quadrature) to our actual stellar measurements. Although of course the tracking motor was turned off, the test setup was actually somewhat sensitive to tower vibration, because the beam from the test lamp was reflected off a mirror attached to the tower. Therefore the 0.05 arcsec figure is an upper limit, and system noise is entirely negligible.

The systematic effects upon our derived values depend largely upon the determination of the peak-to-peak amplitude of the calibration wobbler plate; our estimated uncertainty is $\pm$ 2%. As a check upon the systematics of the differential seeing comparison of the two sites, we have recently interchanged the apparatus between the two, and will accumulate data for six months, then compare and average those results with the first six months' data.

Another assumption that influences the results is the airmass correction of equation (5). As a check we plotted the corrected seeing values against secant Z; a slope not equal to zero would indicate that the slope of the correction was off. No dependence was seen, and we conclude that equation (5) is adequate.

It was our intention originally to include frequencies high enough to avoid large corrections for missing components. Martin (1987) has calculated correction factors to the rms image motion as a function of the windspeed and direction. The relevant parameter is, in his notation, $w\tau/d$, where w is the windspeed, τ is the sampling time of the equipment, and d is the (small) telescope diameter. The median windspeed at Las Campanas is 18 mph, d = 7 inches, and τ = 0.005 sec, so typically $w\tau/d = 0.23$, assuming that the windspeed near the ground is equal to that where the dominant source of turbulence is located. From Martin's (1987) Figure 4 for the case of a single telescope, we see that the transfer of the rms^2 image motion is greater than 98 %, and independent of wind direction. We cannot expect, of course, that the ground layer windspeed is necessarily appropriate in assessing this correction factor. However, the transfer function remains above 90 % even if the relevant windspeed is four times that at the surface. Because we have no independent measurement of τ, this limits the accuracy of our seeing data in an *absolute* sense. Our τ = 0.23 assumption is certainly safe for the differential site comparison however, and will be applied to the final results summarized below.

IV. FIRST RESULTS

We now present some examples of the data, and some of the first results of the production survey which began in October 1988. Two identical systems were set up on two of the most likely locations for the 8-m telescope. Site 2 lies 200 m southeast of the duPont 100-inch telescope dome, and site 3 is located on a peak about a mile to the southeast and at an elevation 100 m higher than site 2. The telescopes, electronics and computer systems are housed in domes 25 feet above ground level. The terrain is smooth all around the

towers; there are no trees. The telescope and mount are bolted to a concrete pedestal that is not physically connected to an outer wind shield which was made from 8-foot diameter culvert pipe. Wind loads on this shield are carried by guy wires which go out some 30 feet from the base of the tower. The operator always points the telescopes away from the wind, and positions the dome so that wind does not hit the telescope directly. This is easy because the wind almost always comes out of the northeast[1]. As it has turned out this seems satisfactory, as we cannot detect windshake in the data. This is straightforward, because the power spectrum of tower vibration has two well-defined peaks at 10 and 17 Hz. If these appear in the power spectrum they can easily be removed.

Figure 5 shows a typical distribution of θ values for one night's worth of data. The values were corrected (on-line) to the zenith, and to 5000 Å according to the equations given above. They were also corrected for the transfer function that rolls off the power spectrum. The distributions represent the summation of roughly 55 histograms produced at a rate of one every ten minutes; data from the two sites refer to the same interval to within about a minute. Six such distributions are recorded each hour. The median value of each distribution is taken to represent the seeing for each ten minute interval. A running mean of three medians was then computed in order smooth the data a little; Figure 6 shows the median seeing in one-half hour intervals, plotted as a function of time throughout the night. We note first that the two sites track each other very well. This gives us considerable confidence in the equipment and in the thermal environments of the two devices, as they are completely independent. It is not yet clear how important seeing effects local to one site or the other are compared to contributions from layers several km above the mountaintop. The rather good correspondence between the two sites seen in Figure 6 is common to virtually all the data we have accumulated so far in the survey, and is clearly a real effect. The correlation between the two sites is so good that one might suspect that much of the image motion is produced by turbulence well above the mountaintop. However, in general the correlation is not perfect, and it seems possible that the similar topography of the two sites causes thermal disturbances to be lifted by the wind into the lightpaths in a manner that is very similar, but not identical, for the two sites.

Figure 7(a) shows the accumulated grand average histogram for all the nights that the systems have been in operation. This graph sums over 61 nights, for a total of 2990 histograms for site 2 (and 2883 for site 3) of 10-minute data blocks. The integral distribution in Figure 7(b) contains the obvious fact that the two sites are indistinguishable on average, as well as the fact that the median seeing at Las Campanas is of order 0.55, at least during the best observing season, from October through April.

There are two caveats to our conclusions about the *absolute* values of the seeing at Las Campanas. First, we are excluding all low frequency components in the calculation of r_o by virtue of our 1 second sampling time. Figure 8 shows a typical average power spectrum of the high frequency motions in the 1 – 256 Hz range for one night; we note that it is still rising below 2 Hz. The average power spectrum of the lowest frequency components, found from the 64 seconds worth of average position data in each 10-minute block were also computed and found to be consistent with the spectrum in Figure 8. At the very lowest frequencies the latter spectrum is not reliable because of tracking errors, but we have

[1] We experimented with double telescope systems on a common mount, in order to discriminate against common-mode signals such as windshake (see Martin 1987). We were not successful in keeping the two systems pointed well enough for several hours, and have temporarily abandoned that approach in order to get some data with one telescope per mount.

no independent way of judging how serious these could be in the north-south direction. Just how one corrects the seeing values estimated from only those components above 2 Hz depends on what one is willing or able to do to correct for slow image motion in one's large telescope. If one could use a tip-tilt system or rapid auto guider (e.g., Thompson and Ryerson 1984) one could perhaps remove frequency components slightly above 2 Hz, and improve the final image quality. This should work a good fraction of the time, because in winds of a few m/s it takes about the same amount of time for a large turbulent element to cross the path of a large and small (seeing) telescope. By combining the average windspeed with the median value of r_o we find that the average coherence time is about 40 msec at 5000 Å. Scaled to 2.2 μm, the average coherence time is 200 msec, which means that in good seeing it should be relatively easy to improve the image quality even with a modest amount of effort.

If one did nothing of the sort to correct for low frequency seeing components, than it might be reasonable to extend the power spectrum to 0.3 Hz. The shape of the power spectrum at low frequencies is approximately $\nu^{-2/3}$, so extension of the power spectrum to 0.3 Hz would add about 7 % to the value of θ. On the other hand, rapid guiding at 5 Hz ought to reduce the θ by about 5 %. Inclusion of frequency components above our cutoff of 200 Hz, say to 500 Hz with the same power law, adds between 5 and 10 % to θ. This correction is quite uncertain because the data show that the power spectrum often steepens above 100 Hz.

Figure 8 illustrates another feature of the power spectra. We grouped the best and worst one-third of the data for the night, averaged the power spectra for these thirds, and normalized them. We note that the poorer seeing data have a very slightly flatter power spectrum on average. This is consistent with the seeing cells being carried across the lightpath systematically faster (due to higher windspeeds) in the poorer seeing data, an intuitively reasonable result. This is generally the case for all the data collected so far.

In summary, we believe that, depending on what one can do in the way of fast guiding, our theoretical large telescope image sizes ought to approach a median value between 0.5 and 0.6 arcseconds FWHM at 5000 Å at the zenith. Table 1 summarizes the medians and quartiles for the first 6 months of data.

We are indebted to a number of people for help in this project: Edward Snoddy and Frank Perez for design of the towers and domes, Ljubo Papic and his crew for tower construction, and our machinists, Lalo Vasquez, Brian Elms, and Pilar Ramirez, who built the instruments. Steve Wilson assisted with the first installation. We also thank Ken Clardy for software and Basil Katem for managing the floppy disk data. The operation of the telescopes was, and continues to be, carried out in expert fashion by Emilio Cerda. Finally, we thank Steve Shectman, Al Hiltner, Buddy Martin, and Nick Woolf for discussions.

Table 1.
Las Campanas Observatory Seeing

fraction	Site 2	Site 3
lower quartile	0.42 (0.47)	0.41 (0.44)
median	0.57 (0.61)	0.55 (0.59)
upper quartile	0.80 (0.86)	0.75 (0.80)

Note: The values are based on 450 hours of data obtained at each site, spread over 61 nights between 1988 October and 1989 April. They refer to FWHM image sizes in arcseconds at 5000 Å at the zenith, as would be expected in a large (perfect) telescope. They have not been corrected for missing low frequency components (below 2 Hz), but the numbers in parentheses have been corrected approximately for missing high frequency components between 200 and 500 Hz. See text for discussion. Two significant digits have been retained to aid in comparing the two sites differentially.

REFERENCES

Angel, J. R. P. 1987, in *Identification, Optimization, and Protection of Optical Telescope Sites*, (Lowell Obeservatory), p. 167.

Babcock, H. W., and Irwin, J. B. 1987, in *Identification, Optimization, and Protection of Optical Telescope Sites*, (Lowell Obeservatory), p. 99.

Forbes, F. F., and Woolf, N. J. 1983, *Proc. SPIE*, **444**, 175.

Fried, D. L. 1965, *J. Opt. Soc. Am.*, **55**, 1427.

Fried, D. L. 1966, *J. Opt. Soc. Am.*, **56**, 1372.

Martin, H. M. 1987, *Pub.A.S.P.*, **99**, 1360.

Moroder, E., and Righini, A. 1973, *Astr.Ap.*, **23**, 307.

Persson, S. E., Babcock, H. W., and Irwin, J. B. 1987, Magellan Project – Las Campanas Site Survey Report No. 3, OCIW internal document.

Sarazin, M., and Roddier, F. 1989, submitted to Astr.Ap..

Thompson, L. A., and Ryerson, H. R. 1984, *Proc. SPIE*, **445**, 560.

Woolf, N. J. 1982, *Ann. Rev. Astr. Ap.*, **20**, 367.

Woolf, N. J., and Ulich, B. L. 1983, in *ESO Workshop on Site Testing for Future Large Telescopes*, ed: A. Ardeberg and L.Woltjer, p. 163.

Young, A. T. 1974, *Ap.J.*, **189**, 587.

FIGURE CAPTIONS

Figure 1. – Schematic of the telescope/seeing monitor. Light from the Questar telescope passes through the calibration plate, reflects off the piezo-mirror, and the bright star is focussed at the knife-edge mirror. Field lenses L1 and L2 image the telescope objective onto the photosurfaces of the photomultiplier tubes PMT1 and PMT2. The output photocurrents produce signal voltages that are first filtered and then compared by the voltage comparator. The calibration plate is driven such that a sinusoidal motion is superimposed upon the stellar image motion at the focus. The eyepiece mirror can be inserted into the beam for acquisition of the star. The guider blade cuts halfway into the beam of PMT2 (in right ascension, which is in and out of the page).

Figure 2. – Schematic timing diagram of the digitization process. The triangle wave (A) that drives the piezo-mirror also represents the motion of a the star across the knife-edge mirror. As the stellar image wanders away from its average position due to seeing (B), the (negative going) outputs of PMT1 and PMT2 (C and D) will turn on (off) sooner or later, as represented by the dotted vertical lines. The crossover points cause the voltage comparator (E) to change state. Counter gate H is generated from these transitions using one-shots (F and G). The gate enables two counters to count 5 MHz clock pulses, N2 and N1. The resulting array of numbers N2 – N1 is linearly proportional to the distance the star is from zero in B.

Figure 3. – Flowchart of the data acquisition processor. See text for description.

Figure 4. – Transfer function of frequency components through the system. The values of r_o and θ are corrected online for this rolloff, out to 200 Hz.

Figure 5. – Sample histogram of a typical night's worth of data: 881025 indicates the night of 1988 October 25. The abscissa is the FWHM of the image as predicted for a large telescope, corrected for transfer function and converted to an airmass of unity and 5000 Å. The vertical tick mark indicates the median, which happens to be the same for the two sites on this night. The frequency range is 2 – 200 Hz, so slow motion seeing components are absent. The light and heavy lines show the results for the two sites, which are in operation simultaneously. Histograms analogous to these are produced and recorded every ten minutes.

Figure 6. – Time variation through the night of the median seeing in each half-hour during the night of 1988 October 25. The ordinate is the running average of three medians found from the 10-minute histograms (like Figure 5).

Figure 7. – Like Figure 5, but for all 61 nights added together. The integral distribution in figure 7(b) shows the fraction of the time that the seeing is *better* than the ordinate value. The quartiles and median read from this graph are given in Table 1.

Figure 8. – Average high frequency power spectrum of a typical night's data. The best and worst one-third of the data (labelled 'b' and 'w' respectively) have been averaged separately to look for differences in slope; the offset between them has been removed and the level has been arbitrarily set to zero at 10 Hz. The spectra for site 3 have been offset by 20 db for clarity. Note that slightly more energy is present at higher frequencies when the seeing is worse. Generally the power spectra from the two sites are well correlated, as illustrated here.

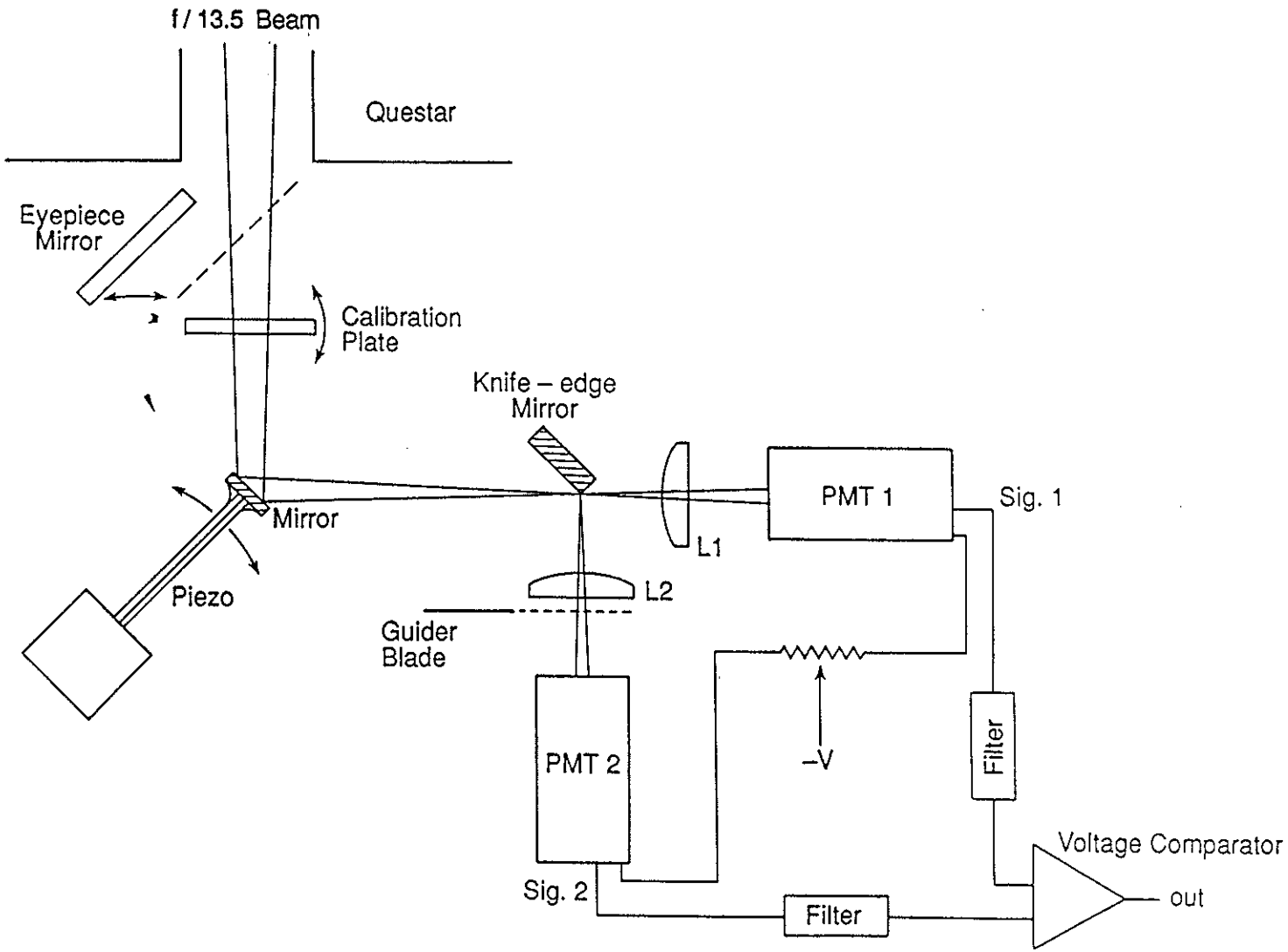
f / 13.5 Beam
Questar
Eyepiece Mirror
Calibration Plate
Knife – edge Mirror
Mirror
Piezo
L1
L2
PMT 1
Sig. 1
Guider Blade
PMT 2
–V
Filter
Voltage Comparator
Sig. 2
Filter
out

Figure 1

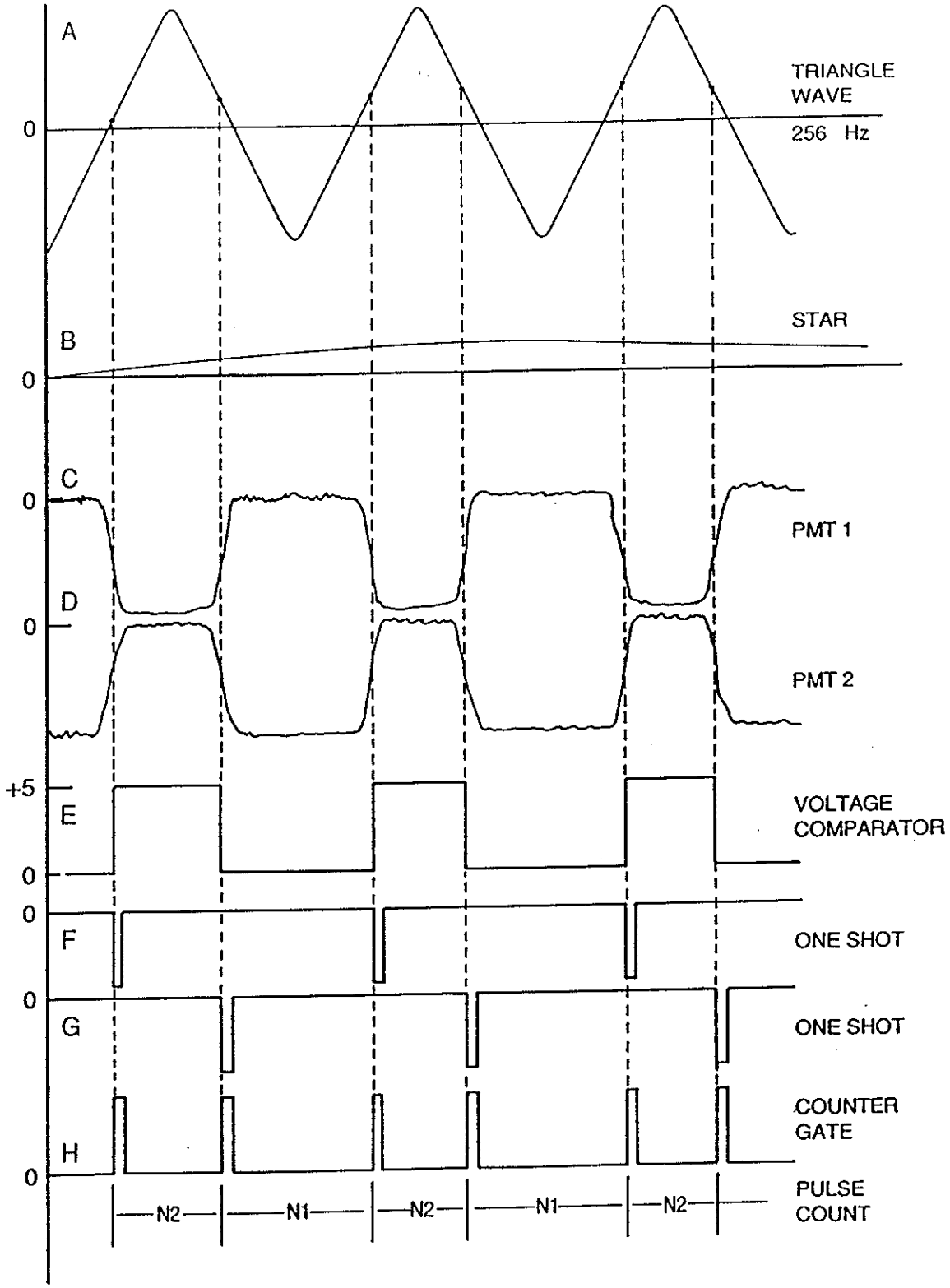
A
TRIANGLE
WAVE
0
256 Hz
STAR
B
0
C
0
PMT 1
D
0
PMT 2
+5
E
VOLTAGE
COMPARATOR
0
0
F
ONE SHOT
0
G
ONE SHOT
COUNTER
GATE
H
0
N2
N1
N2
N1
N2
PULSE
COUNT

Figure 2

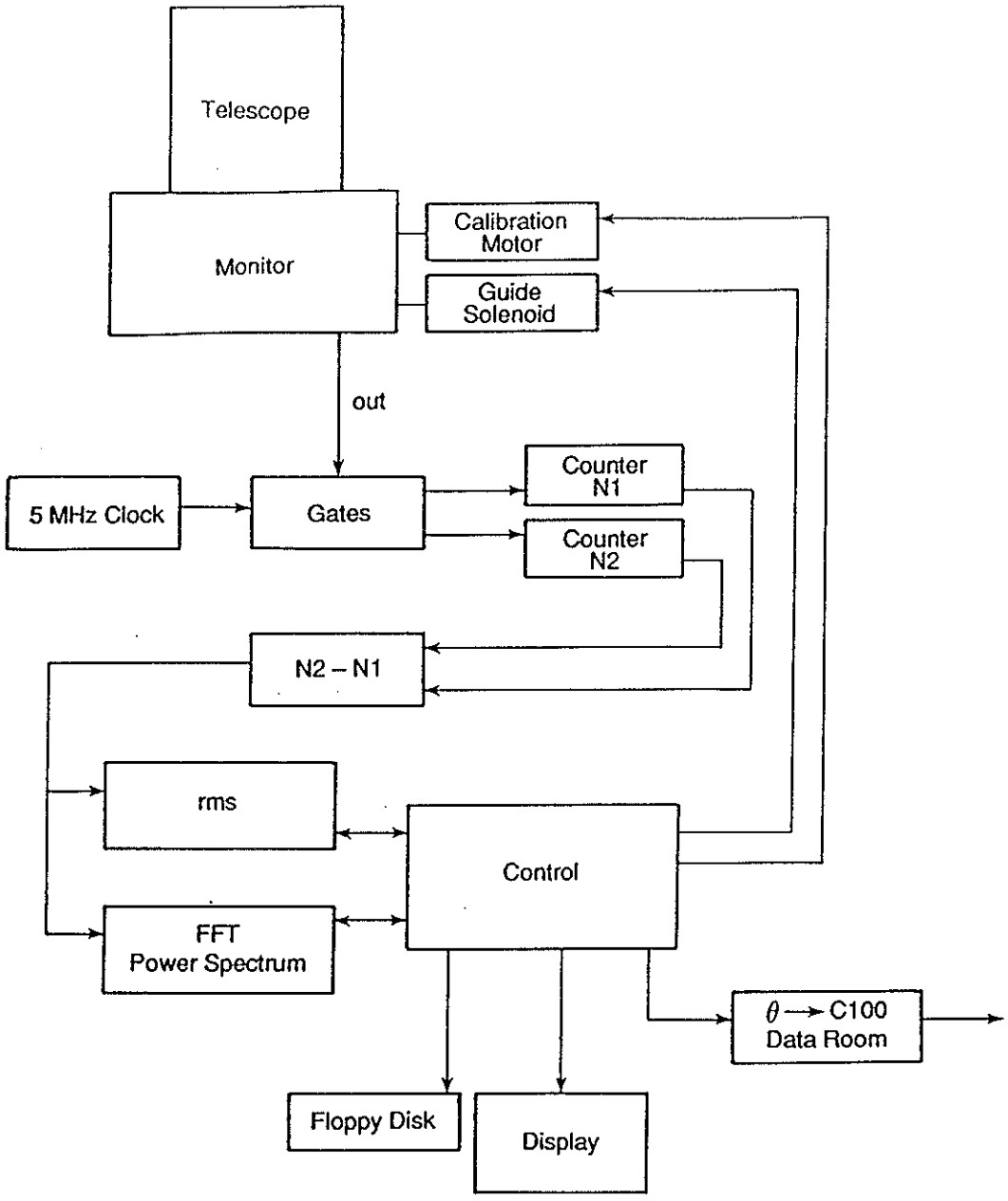
Telescope
Monitor
Calibration Motor
Guide Solenoid
out
5 MHz Clock
Gates
Counter N1
Counter N2
N2 – N1
rms
Control
FFT Power Spectrum
θ → C100 Data Room
Floppy Disk
Display

Figure 3

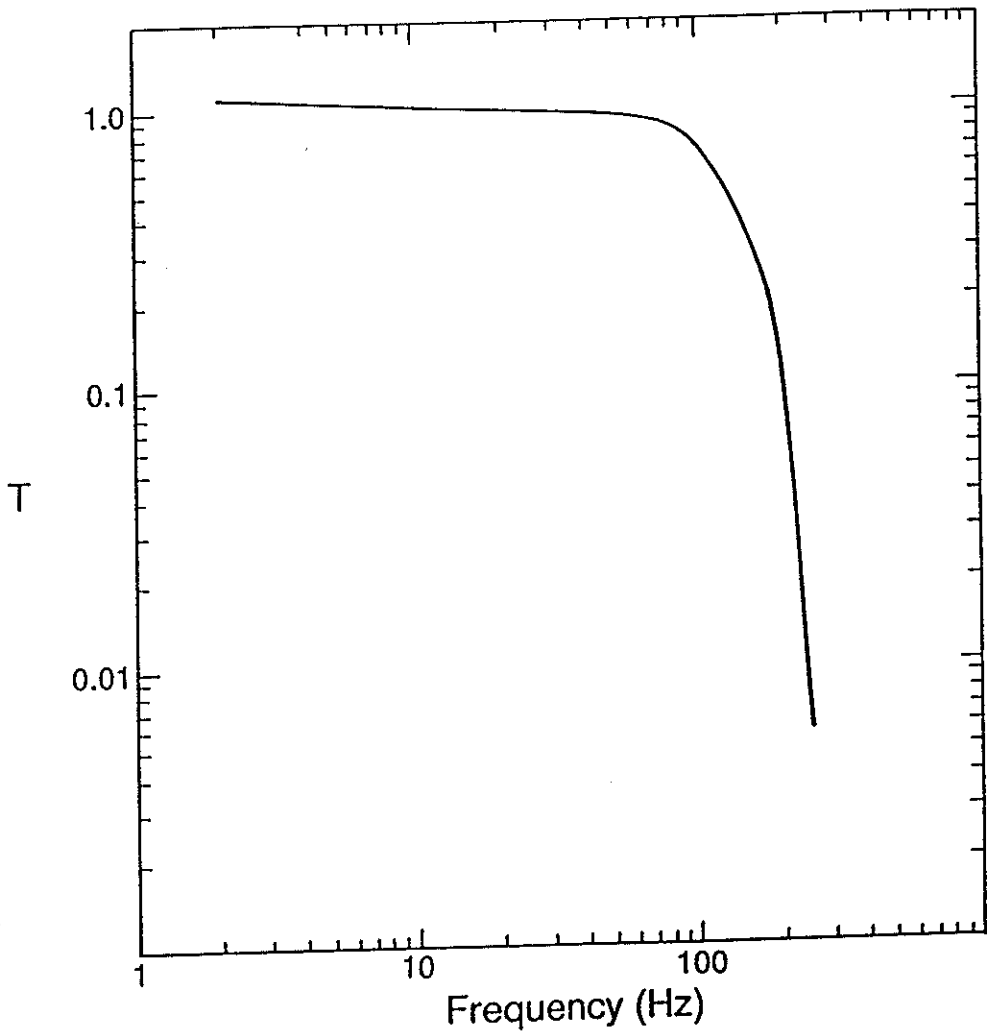

Figure 4

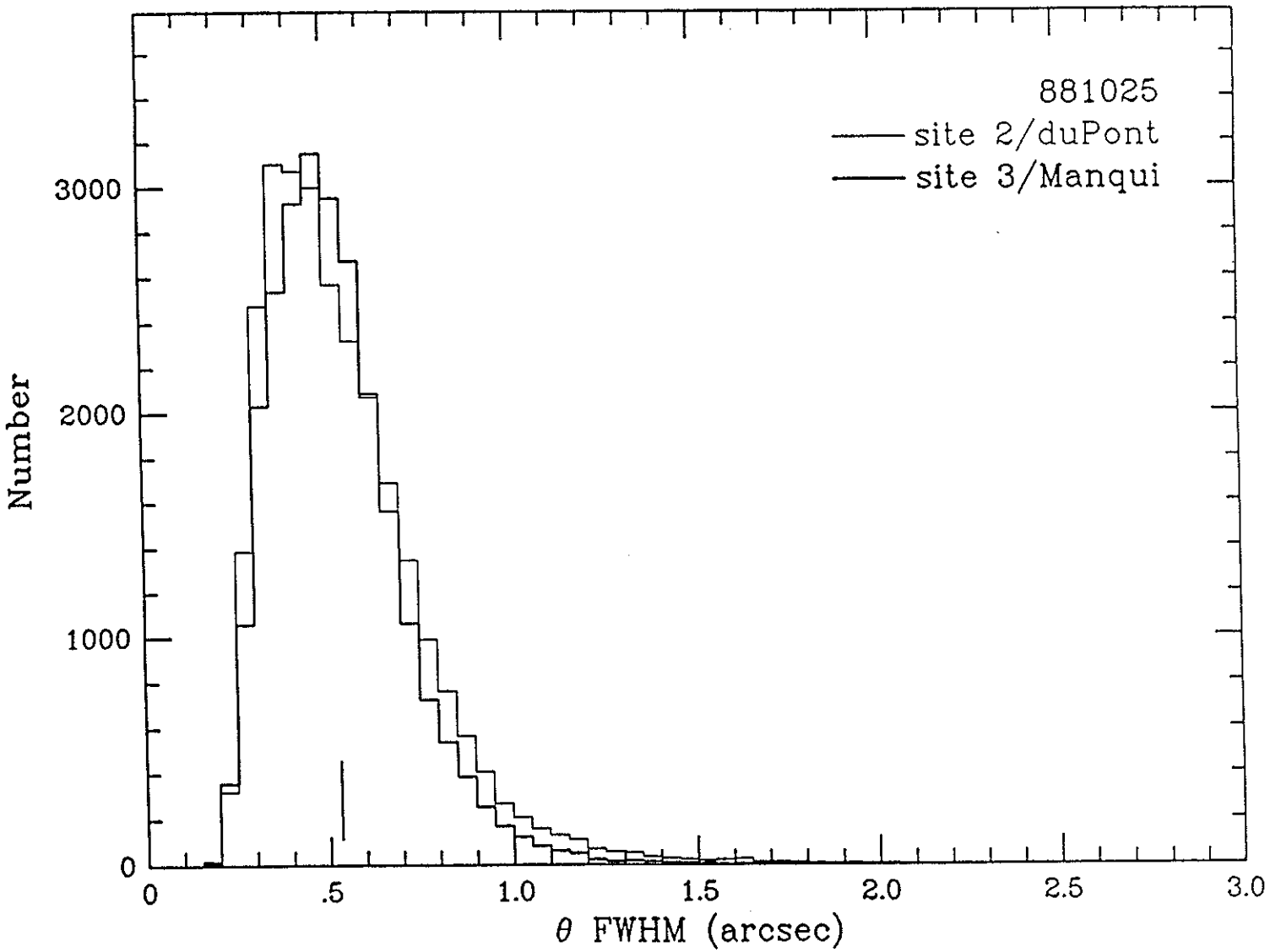
881025
site 2/duPont
site 3/Manqui
Number
3000
2000
1000
0
0
.5
1.0
1.5
2.0
2.5
3.0
θ FWHM (arcsec)

Figure 5

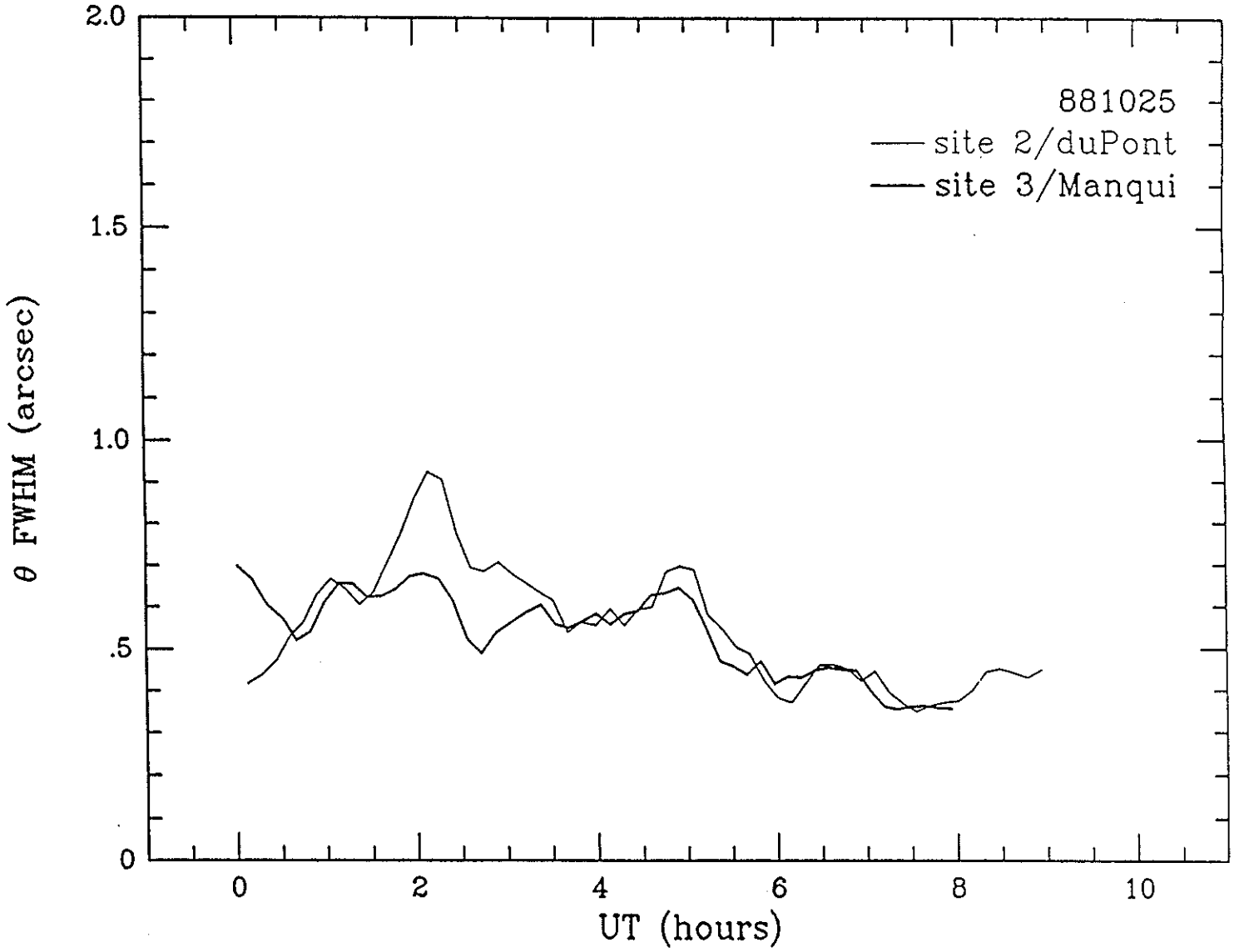
2.0
1.5
1.0
.5
0
θ FWHM (arcsec)
0
2
4
6
8
10
UT (hours)
881025
site 2/duPont
site 3/Manqui

Figure 6

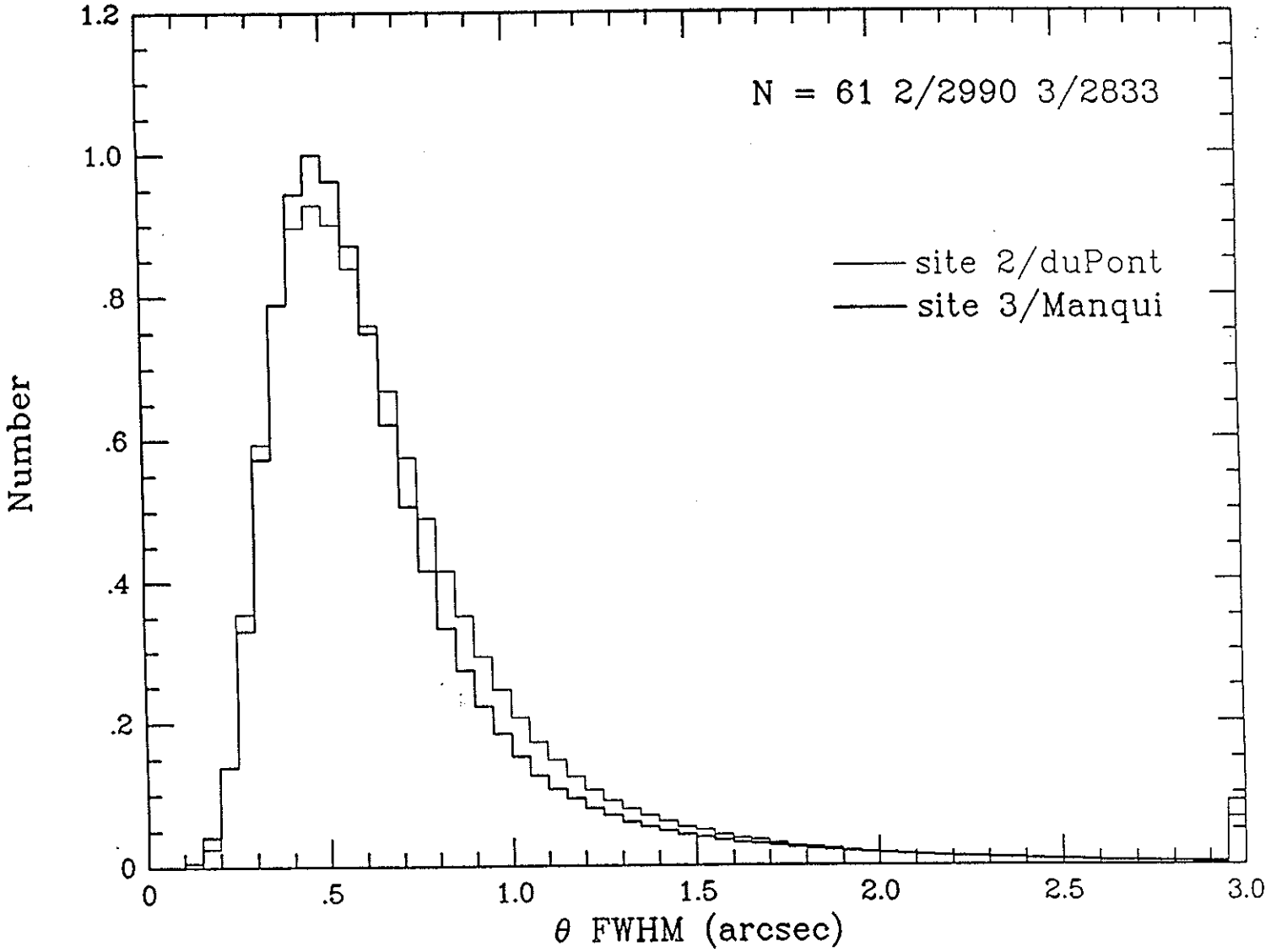
N = 61 2/2990 3/2833
site 2/duPont
site 3/Manqui
Number
θ FWHM (arcsec)
1.2
1.0
.8
.6
.4
.2
0
0
.5
1.0
1.5
2.0
2.5
3.0

Figure 7(a)

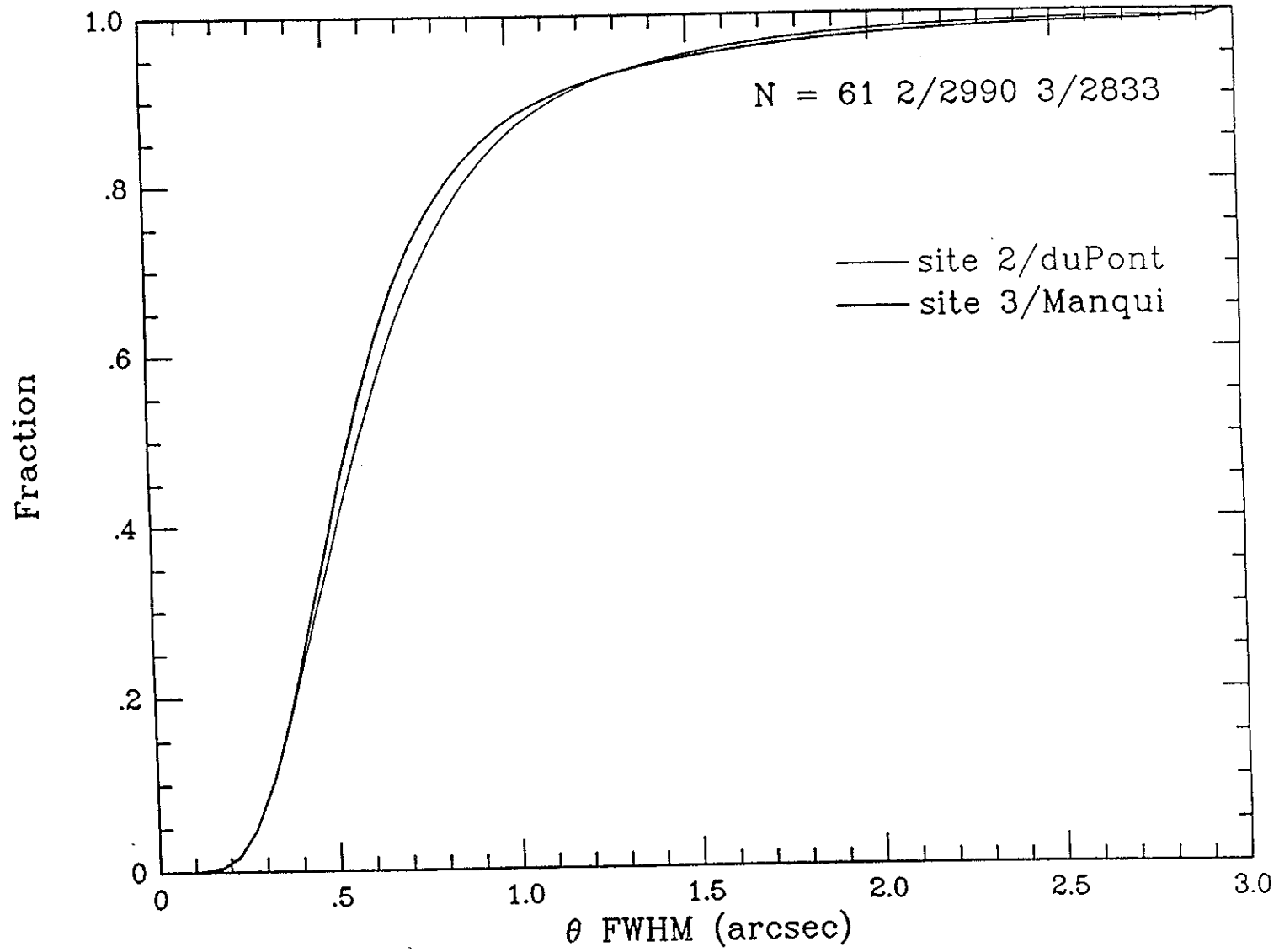
1.0
.8
.6
.4
.2
0
Fraction
N = 61 2/2990 3/2833
site 2/duPont
site 3/Manqui
0
.5
1.0
1.5
2.0
2.5
3.0
θ FWHM (arcsec)

Figure 7(b)

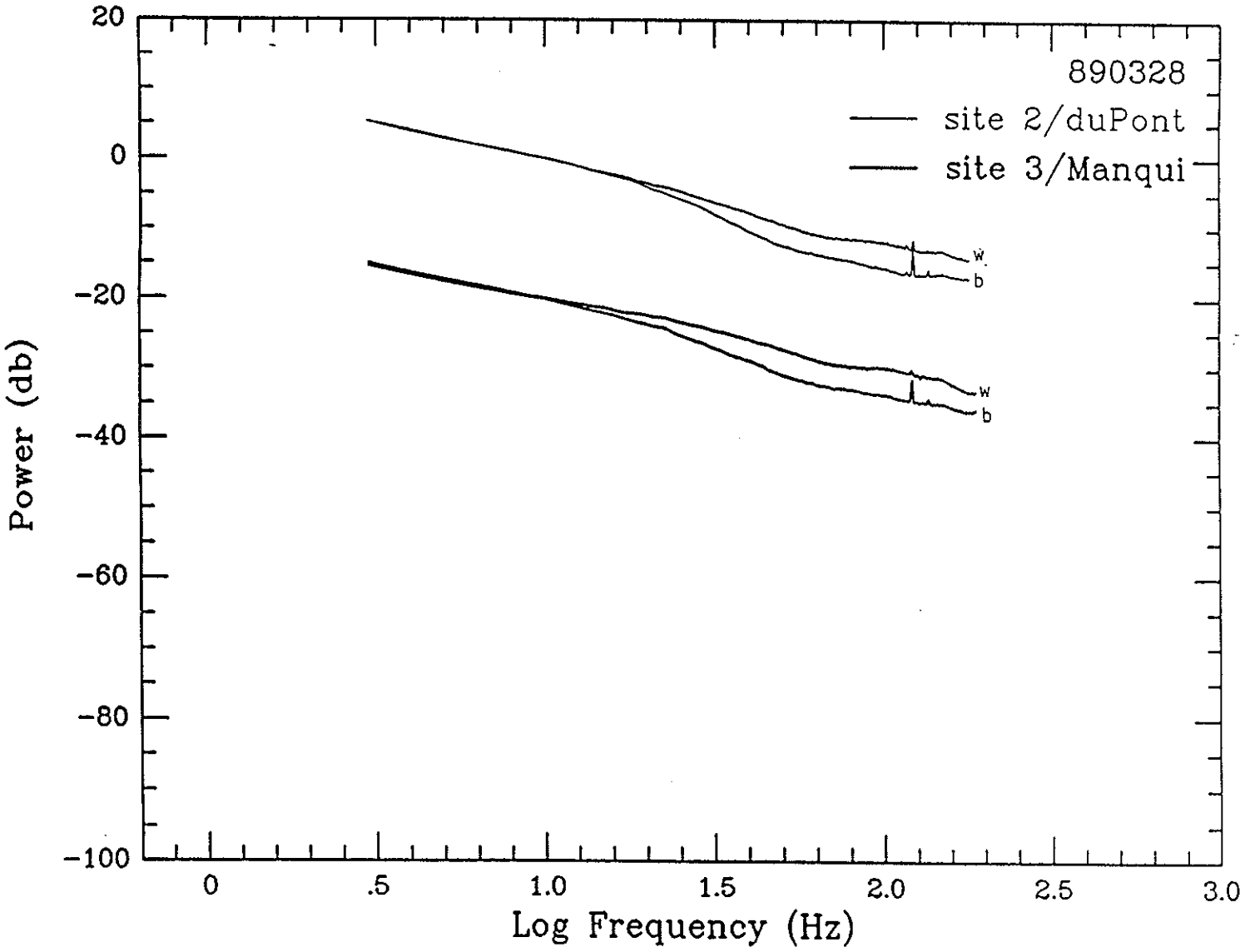
890328
site 2/duPont
site 3/Manqui
w
b
w
b
20
0
-20
-40
-60
-80
-100
Power (db)
0
.5
1.0
1.5
2.0
2.5
3.0
Log Frequency (Hz)

Figure 8